# Impact of Li addition in Al-rich alloys for hydrogen production in water

Tiantian He [a], Yi Xiong [b], Sanming Du [a, b], Zhenjun Yuan [a], Xinyu Liang [b], Marko Huttula [c], Wei Cao [c,d]

[a] National United Engineering Laboratory for Advanced Bearing Tribology, Henan University of Science and Technology, Luoyang 471023, China

[b] School of Materials Science and Engineering, Henan University of Science and Technology, Luoyang 471023, China

[c] Nano and Molecular Systems Research Unit, University of Oulu, FIN-90014, Finland

[d] School of Mechanical and Automotive Engineering, Anhui Polytechnic University, Wuhu 241000, Anhui, China

Corresponding author. Tel.: +86 379 64231723; fax: +86 379 64231723.

E-mail address: tthe@haust.edu.cn (Tiantian He)

**Abstract:** In this study, three types of aluminum alloys (Al-Li, Al-Ga-In-Sn, Al-Li-Ga-In-Sn alloys) were prepared via vacuum arc melting technology. The microstructures of the alloys were examined by X-ray diffraction (XRD), scanning electron microscopy (SEM) and energy dispersive spectroscopy (EDX). The water discharge method was used to evaluate the water-aluminum reaction. The results show that the Al-Li alloy is inert in aqueous ambience, whereas the Al-Ga-In-Sn alloy and Al-Li-Ga-In-Sn alloy rapidly react with water. Meanwhile, the Li addition hinders the aluminum-water reaction mainly due to the formation of AlLi and $Li_5Sn_2$ intermetallic compounds, which causes a lower $H_2$ generation rate and a lower $H_2$ yield of Al-Li-Ga-In-Sn alloys than that of the Al-Ga-In-Sn alloy.

**Key words:** Al-rich alloy, low melting point phase, microstructure, aluminum-water reaction.

## 1. Introduction

Hydrogen is widely accepted as a renewable and ideal fuel, due to its high caloric content, abundant resources, and environmental friendly features [1-5]. Currently, it is considered a future alternative of the conventional fossil fuel. However, the hydrogen production, safe storage, transportation, and delivery limit the hydrogen value chain and applications. At present, the generation of hydrogen by the hydrolysis of metal or metal hydrides has attracted much attention from scientists [6-11]. Among the available methods, Al metal or alloys can directly generate hydrogen from

water due to its high energy storage, light weight, natural abundance, environmental safety of the reaction products, and low cost. However, the stable alumina film on the Al surface prevents the Al-water reaction. Thus, high temperature is normally required for the reaction [12-20].

To circumvent the blockages of the passive oxide on Al, the metal was alloyed with low melting point counterparts such as Ga, In and Sn [21-23]. Woodall [24] suggested that the Al-Ga-In-Sn alloy has considerable reactivity. It can directly react with the water under normal conditions, and these alloys yield higher reactivity. The intermetallic compounds formed with Ga, In and Sn at the grain boundary prevent the Al passivation, and provide transportation routes of Al to reach the reaction sites. As a result, the reaction process is repeated until most or all of Al atoms are consumed by the reaction. In recent years, Wang et al. [25-28] prepared Al-Ga-In-Sn quaternary alloys with different compositions by using the traditional smelting process (arc melting and induction melting), and studied the microstructure and phase composition of alloys, including the melting point of Ga-In-Sn (GIS) phase. A low melting point Ga-In-Sn phase in alloys was identified with a melting point near 10.7 °C, which further demonstrated the mechanism of the Al-water reaction proposed by Woodall. Meanwhile, the $H_2$ evolution rate was found to be closely relevant to the microstructure of alloys. The size of the Al grains and the composition, size and number of the Ga-In-Sn phase are the key factors to control the reaction rate of Al and water. These works provide a preliminary research background of the relationship between the microstructure, composition, preparation process and the Al-water reaction of alloys. However, in practical applications, the reaction temperature, reaction rate and $H_2$ yield of Al-water gain are also key factors for hydrogen production. For example, if hydrogen is used as a portable energy source, the reaction temperature and $H_2$ generation rate must be controlled. Therefore, it is necessary to find the key factors and rules to control the Al-water reaction.

It is well known that the chemically active Li metal can vigorously react with water to produce hydrogen. Due to its light weight, it has a high hydrogen storage capacity. Therefore, the addition of Li to the Al-rich alloy may accelerate the Al-water reaction. In addition, Li and Al may form intermetallic compounds such as AlLi, $Al_2Li_3$ and

$Al_4Li_9$. These intermetallic compounds precipitate on the aluminum grain boundaries, which affect the formation and distribution of GIS phases. The Al-water reaction is inevitably affected when the direct contact between the Al grains and the GIS phases is cut off by these compounds.

In this paper, Al-Li, Al-Ga-In-Sn and Al-Li-Ga-In-Sn alloys were prepared by vacuum arc melting technology. The microstructure and phase composition of Al-Li, Al-Ga-In-Sn and Al-Li-Ga-In-Sn alloys were systematically studied, and the Al-water reaction of alloys at different water temperatures was investigated. The effect of alloying element Li on the hydrolysis of aluminum alloy was explored. The mechanism of hydrogen production by the hydrogenation of the aluminum alloy was revealed, and the composition ratio of aluminum alloy was further optimized. The results serve as a theoretical and experimental starting point for the control of the Al-water reaction and broaden the practical application of the alloy.

## 2. Experimental details

The Al-Li, Al-Ga-In-Sn and Al-Li-Ga-In-Sn alloys were synthesized by arc-melting. The nominal compositions of the alloy ingots are shown in Table 1. The charging materials are industrial pure Al and Li with over 99.9 wt.% purity of Ga, In and Sn. The alloy ingots (40 g in mass) were melted in a high-purity argon atmosphere in a water-cooled copper crucible several times to ensure the compositional homogeneity.

The phase compositions of the alloys were analyzed by X-ray diffraction (XRD) using a Rigaku D/max 2400 diffractometer with monochromated CuKα radiation (kα1=0.154056 nm). The microstructures of alloys were characterized using an FEI Inspect F50 scanning electron microscope (SEM) with a Quanta 600 EDX (Energy Dispersed X-ray) system. The fracture surfaces of samples were observed. To minimize the oxidation of the fresh fracture surface, all samples were placed into the sample chamber as soon as they were broken.

The water displacement method was used to measure the hydrogen generation rate of alloys. The equipment in the $H_2$ generation is similar to that described in a previous study [27]. The sample was dropped into a 250 ml Pyrex glass reactor (containing distilled water) on a water bath. The weight of the ejected water due to the $H_2$ release was

automatically recorded using a one ten-thousandth scale. The data and reaction time were stored in a computer. After the calibration of the recorded weight of ejected water, the water mass was converted to $H_2$ generated volume under the standard conditions (273 K, 1 atm) using the ideal gas equation. The added mass was approximately 0.3 g for each experiment. The temperature of experiments was maintained constant at 20 °C, and the humidity was below 20%.

## 3. Results and discussion

### 3.1 XRD analysis

Fig. 1 shows the XRD patterns of Al-2Li, Al-6GIS, Al-2Li-6GIS alloys. All samples contain an Al (Ga) solid solution as a result of the partial dissolution of Ga into Al lattices. The AlLi phase is found in the Al-2Li alloy. According to the Al-Li binary phase diagram, when the Li content is higher than 5 wt.%, the AlLi phase is formed due to the eutectic reaction [29]. However, a water-cooled copper crucible was used for alloy cooling in the present work. Thus, the formation of the AlLi phase in the Al-2Li alloy is mainly attributed to the nonequilibrium rapid solidification. Meanwhile, an $In_3Sn$ phase is found in the Al-6GIS alloy. The Al-2Li-6GIS alloy contains AlLi, $In_3Sn$ and $Li_5Sn_2$ phases. Moreover, the diffraction peaks of the AlLi phase in the Al-2Li-6GIS alloy are stronger than that in the Al-2Li alloy, mainly because some Ga is dissolved into Al lattices in the Al-2Li-6GIS alloy, which reduces the solid solution degree of Li in Al and yields more AlLi.

### 3.2 SEM observations

Fig. 2 shows the typical SEM morphologies of Al-2Li, Al-6GIS, Al-2Li-6GIS alloys. Due to a small load of Li in the Al-2Li alloy, the fracture morphology shows many dimples with an average size of 42±24 μm, as observed in Figs. 2a and b. Meanwhile, few bright white AlLi intermetallic compounds are precipitated near the dimple (Fig. 2 b). From Figs. 2c and d, the fracture morphology of the Al-6GIS alloy is a typical columnar structure with an average Al grain size (columnar width) of approximately 55±26 μm. Some bright white $In_3Sn$ phases are also found on the surface of the alloy. In Fig. 2e and f, Al grains of the Al-2Li-6GIS alloy remain columnar, which shows an obvious directional growth during the alloy solidification. However, compared with the grain in the Al-6GIS alloy, the present grain is

shorter in length and wider in width (106±26μm) as shown in Fig. 2e. Figs. 2e and f also show that many bright white $In_3Sn$ and AlLi precipitates are distributed on the surface of the alloy.

The phase composition of the alloy was analyzed by EDX, and the results are shown in Table 2. No Li was observed in the Al-2Li alloy or Al-2Li-6GIS alloy mainly due to the EDX detection limits of the light elements below C. For the Al-6GIS and Al-2Li-6GIS alloys, a small amount of Ga is found in Al grains. In addition to Al and Ga, intensive O is observed in the fracture after the oxidization of Al-6GIS and Al-2Li-6GIS alloys. For the Al-6GIS and Al-2Li-6GIS alloys, both In and Sn elements are observed in the bright white particles at the Al grain boundaries (GB). In combination to the XRD results, the bright white precipitation on the GB of the alloy contains the $In_3Sn$ phase. However, the atomic ratio of In:Sn approaches 1.7:1 (Al-6GIS alloy) and 6:1 (Al-2Li-6GIS alloy), which deviates from 3:1 and suggests that those phases also contain extra In or Sn in addition to $In_3Sn$.

3.3 Reactivity of alloys with water

The Al-2Li alloy did not react with water because there was a passive oxidization layer on the Al surface. However, once the Al-6GIS and Al-2Li-6GIS alloys contacted water, the alloys immediately reacted with water, and $H_2$ bubbles began to incessantly flow from water. Fig. 3 shows the typical $H_2$ production curves of Al-6GIS and Al-2Li-6GIS alloys at different water temperatures. The $H_2$ generation rates and $H_2$ yields of alloys were calculated from Fig. 3, and they are plotted in Fig. 4 and tabulated in Table 3. As shown in Fig. 3, the $H_2$ generation rate and $H_2$ yield of the Al-6GIS alloy are higher than those of the Al-2Li-6GIS alloy at the same temperature. At 50 °C water temperature, the Al-water reaction lasted approximately 200 min. The $H_2$ yield of the Al-6GIS alloy is nearly 86%. For the Al-2Li-6GIS alloy, the reaction time is about 480 min and the $H_2$ yield is 84%. At 70 °C, the reaction times of the Al-6GIS alloy and Al-2Li-6GIS alloy are approximately 125 min and 225 min, respectively. The $H_2$ yields of both alloys reach 100%. The results in Fig. 3 also demonstrate the importance of the water temperature during the Al-water reaction. The $H_2$ generation rate and $H_2$ yield increase with the reaction temperature.

The Li addition reduces the $H_2$ generation rate of the Al-6GIS alloy. As given in Fig. 4, the maximum $H_2$

generation rates are 13 ml/min·g Al and 10 ml/min·g Al for the Al-6GIS alloy and Al-2Li-6GIS at 50 °C, respectively. When the water temperature is 60 °C, the value increases to 27 ml/min·g Al and 15 ml/min·g Al. When the water temperature further increases to 70 °C, the maximum $H_2$ generation rate of the Al-6GIS alloy and Al-2Li-6GIS alloy are 37 ml/min·g Al and 17 ml/min·g Al. Thus, the Li addition hinders the Al-water reaction of the alloy, which causes a decrease in $H_2$ generation rate and $H_2$ yield. From the microstructure analysis, Li forms two intermetallic compounds AlLi and $Li_5Sn_2$ on the Al grain boundaries, which affect the formation and distribution of GIS phases, inhibits the Al-water reaction, and causes the decrease in the $H_2$ generation rate and $H_2$ yield.

### 3.4 Byproducts of the reactions

Fig. 5 shows the XRD patterns of the byproducts of Al-6GIS alloy and Al-2Li-6GIS alloy after the reaction with water at 60 °C. The lack of LiOH phase in the figure indicates that Li does not react with water. The byproducts of the Al-water reaction of the alloy are mainly $Al(OH)_3$ and AlO(OH). As shown in Fig. 5, the Al-2Li-6GIS alloy has more $Al(OH)_3$ but less AlO(OH) than the Al-6GIS alloy, because the Al-6GIS alloy has a higher reaction rate, which generates substantial heat, and causes a rapid increase in local water temperature in favor of the AlO(OH) formation. Therefore, with the increase in water temperature, the byproducts of the Al-water reaction of the Al alloy gradually changes from $Al(OH)_3$ to AlO(OH), which is consistent with the results of A.V. Ilyukhina [30]. They found that when the water temperature was below 25 °C, the byproduct was $Al(OH)_3$. When the water temperature was increased from 40 °C to 60 °C, the byproduct became a mixture of $Al(OH)_3$ and AlO(OH). The amount of $Al(OH)_3$ decreased with the reaction temperature, whereas the amount of AlO(OH) increased. When the temperature was over 60 °C, the byproduct was AlO(OH). The $In_3Sn$ phase is also detected in Fig. 5, which indicates that the low melting point metal does not react with water but only provides a passage for the Al-water reaction.

## 4. Conclusions

To conclude, the Li addition has great effects on the phase composition of Al-Li-Ga-In-Sn alloys. $In_3Sn$, AlLi and $Li_5Sn_2$ phases precipitate at the Al grain boundaries. Corresponding to the microstructures of alloys, the Li addition

hinders the Al-water reaction of the alloy and reduces the $H_2$ generation rate and yield. This phenomenon is attributed to AlLi and $Li_5Sn_2$ on the Al grain boundaries, which affect the formation and distribution of GIS phases. As a result, Al slowly reacts with water and some Al remains without consumption. In addition, the water temperature greatly affects the byproducts of the Al-water reaction. With the increase in water temperature, the byproducts of the Al-water reaction of the Al alloy gradually changes from $Al(OH)_3$ to AlO(OH).

**Acknowledgments**

This work was financially supported by National Natural Science Foundation of China (Grant No. 51171201), National Basic Research Program of China (2010CB631305), the Key Scientific Research Projects in Henan Province (18B430007), the Academy of Finland (Grant No. 311934), the Program for Science, Technology Innovation Talents in Universities of Henan Province (17HASTIT026), Education Department of Henan Province (16A430005) and the Science and Technology Innovation Team of Henan University of Science and Technology (2015XTD006).

**References**

[1] S.H. Mohr, J. Wang, G. Ellem, J. Ward, D. Giurco, Projection of world fossil fuels by country, Fuel, 2015 (141): 120-135.

[2] N. Muradov, Low-carbon production of hydrogen from fossil fuels, Compendium of Hydrogen Energy, 2015: 489-522.

[3] G. Nicoletti, N. Arcuri, G. Nicoletti, R. Bruno, A technical and environmental comparison between hydrogen and some fossil fuels, Energy Conversion and Management, 2015 (89): 205-213.

[4] M. Ball, M. Weeda, The hydrogen economy-Vision or reality?, Compendium of Hydrogen Energy, 2016 (4): 237-266.

[5] S. Dutta, A review on production, storage of hydrogen and its utilization as an energy resource, Journal of Industrial and Engineering Chemistry, 2014 (20): 1148-1156.

[6] X.Y. Chen, Z.W. Zhao, M.M. Hao, D.Z. Wang，Hydrogen generation by splitting water with Al-Li alloys, International

Journal of Energy Reaserch, 2013, 37(13): 1624-1634.

[7] S.K. Oh, M.J. Kim, K.S. Eom, J.S. Kyung, D.H. Kim, E.A. Cho, H.S. Kwon, Design of Mg-Ni alloys for fast hydrogen generation from seawater and their application in polymer electrolyte membrane fuel cells, International Journal of Hydrogen Energy, 2016 (41): 5296-5303.

[8] S. Liu, M.Q. Fan, C.Wang, Y.X. Huang, D. Chen, L.Q. Bai, K.Y. Shu , Hydrogen generation by hydrolysis of Al-Li-Bi-NaCl mixture with pure water, International Journal of Hydrogen Energy, 2012, 37(1):1014-1020.

[9] F. Xu, L.X. Sun, X.F. Lan, H.L. Chu, Y.J. Sun, H.Y. Zhou, F. Li, L.N. Yang, X.L. Si, J. Zhang, S. Walter, Z. Gabelica, Mechanism of fast hydrogen generation from pure water using Al-$SnCl_2$ and bi-doped Al-$SnCl_2$ composites, International Journal of Hydrogen Energy, 2014 (39): 5514-5521.

[10] Z.Y. Deng, Y.B. Tang, L.L. Zhu, Y. Sakka, J. Ye, Effect of different modification agents on hydrogen-generation by the reaction of Al with water, International Journal of Hydrogen Energy, 2010 (35): 9561-9568.

[11] L. Soler, A.M. Candela, J. Macanás, M. Muñoz, J. Casado, Hydrogen generation from water and aluminum promoted by sodium stannate, International Journal of Hydrogen Energy, 2010 (35): 1038-1048.

[12] X.Y. Chen, Z.W. Zhao, X.H. Liu, M.M. Hao, A.L. Chen, Z.Y. Tang, Hydrogen generation by the hydrolysis reaction of ball-milled aluminium-lithium alloys, Journal of Power Sources, 2014,254:345-352.

[13] H. Wang, Y. Chang, S. Dong, Z. Lei, Q. Zhu, P. Luo, Z. Xie, Investigation on hydrogen production using multicomponent aluminum alloys at mild conditions and its mechanism, International Journal of Hydrogen Energy, 2013 (38): 1236-1243.

[14] M.Q. Fan, L.X. Sun, F. Xu, D.S. Mei, D. Chen, W.X. Chai, F.L. Huang, Q.M. Zhang, Microstructure of Al-Li alloy and its hydrolysis as portable hydrogen source for proton-exchange membrane fuel cells, International Journal of Hydrogen Energy, 2011, 36(16):9791-9798

[15] Y.Y. Jia, J. Shen, H.X. Meng, Y.M. Dong, Y.J. Chai, N. Wang, Hydrogen generation using a ball-milled Al/Ni/NaCl mixture, Journal of Alloys and Compounds, 2014, 588: 259-264.

[16] H. Zou, S. Chen, Z. Zhao, W. Lin, Hydrogen production by hydrolysis of aluminum, Journal of Alloys and Compounds, 2013 (578): 380-384.

[17] A.O. Dudoladov, O.A. Buryakovskaya, M.S. Vlaskin, A.Z. Zhuk, E.I. Shkolnikov, Generation of hydrogen by aluminium oxidation in aquaeous solutions at low temperatures, International Journal of Hydrogen Energy, 2016 (41): 2230-2237.

[18] Y.A. Liu, X.H. Wang, H.Z. Liu, Z.H. Dong, S.Q. Li, H.W. Ge, M. Yan, Effect of salts addition on the hydrogen generation of Al-LiH composite elaborated by ball milling, Energy, 2015 (89): 907-913.

[19] M.Q. Fan, S. Liu, C. Wang, D. Chen, K.Y. Shu, Hydrolytic hydrogen generation using milled aluminum in water activated by Li, In, and Zn additives, 2012, 12(4):642-648.

[20] H.B. Dai, G.L. Ma, H.J. Xia, P. Wang, Reaction of aluminium with alkaline sodium stannate solution as a controlled source of hydrogen, Energy and Environmental Science, 2011 (4): 2206-2212.

[21] J.T. Ziebarth, R. Kramer, J. Woodall, D. Sherman, G. Choi, C. Allen, J. Jeon, Splitting water with Al rich alloys: structure and reaction Kinetics, in: Meeting Abstracts, The Electrochemical Society, 2008, pp. 661-661.

[22] J.T. Ziebarth, J.M. Woodall, R.A. Kramer, G. Choi, Liquid phase-enabled reaction of Al-Ga and Al-Ga-In-Sn alloys with water, International Journal of Hydrogen Energy, 2011 (36): 5271-5279.

[23] J. Woodall, J.T. Ziebarth, C.R. Allen, D.M. Sherman, J. Jeon, G. Choi, Recent results on splitting water with aluminum alloys, Ceram Trans, 2009 (202): 121-127.

[24] J.M. Woodall, J. Ziebarth, C.R. Allen, The science and technology of Al-Ga alloys as a material for energy storage, transport, and splitting water, in: Proceedings of the ASME 2nd energy nanotechnology international conference, 2007.

[25] W. Wang, D.M. Chen, K. Yang, Investigation on microstructure and hydrogen generation performance of Al-rich alloys, International Journal of Hydrogen Energy, 2010 (35): 12011-12019.

[26] W. Wang, W. Chen, X.M. Zhao, D.M. Chen, K. Yang, Effect of composition on the reactivity of Al-rich alloys

with water, International Journal of Hydrogen Energy, 2012 (37): 18672-18678.

[27] T.T. He, W. Wang, D.M. Chen, K. Yang, Reactivity of Al-rich alloys with water promoted by liquid Al grain boundary phases, Journal of Materials Science and Technology, 2017, 33: 397-403.

[28] W. Wang, X.M. Zhao, D.M. Chen, K. Yang, Insight into the reactivity of Al-Ga-In-Sn alloy with water, International Journal of Hydrogen Energy, 2012 (37): 2187-2194.

[29] N.E. Prasad, T.R. Ramachandran, Chapter 3: Phase diagrams and phase reactions in Al-Li, Alloys Aluminum-lithium Alloys, 2014, 61-97.

[30] A.V. Ilyukhina, O.V. Kravchenko, B.M. Bulychev, E.I. Shkolnikov, Mechanochemical activation of aluminm with gallams for hydrogen evolution from water, International Journal of Hydrogen Energy, 2010 (35): 1905-1910.

## Table captions:

Table 1 Nominal compositions of the prepared alloy ingots (wt.%).

Table 2 Compositions of the alloys obtained using EDX.

Table 3 $H_2$ yields of the alloys at different water temperatures (%).

## Figure captions:

Fig. 1 XRD patterns of different alloys.

Fig. 2 Fracture surfaces of different alloys: (a), (b) Al-2Li alloy; (c), (d) Al-6GIS alloy; (e), (f) Al-2Li-6GIS alloy.

Fig. 3 $H_2$ production curves of the Al-6GIS alloy and Al-2Li-6GIS alloy measured at different water temperatures: (a) 50 °C; (b) 60 °C; (c) 70 °C.

Fig. 4 $H_2$ generation rates of the alloys at different water temperatures.

Fig. 5 XRD patterns of the byproducts of the Al-6GIS alloy and Al-2Li-6GIS alloy after the reaction with water at 60 °C.

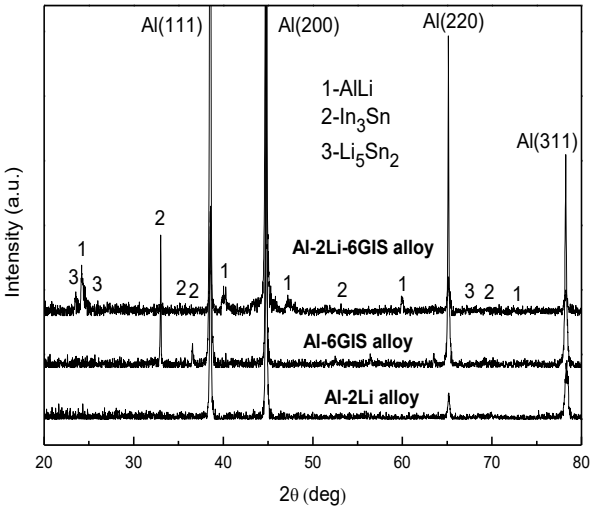


Fig. 1 XRD patterns of different alloys.

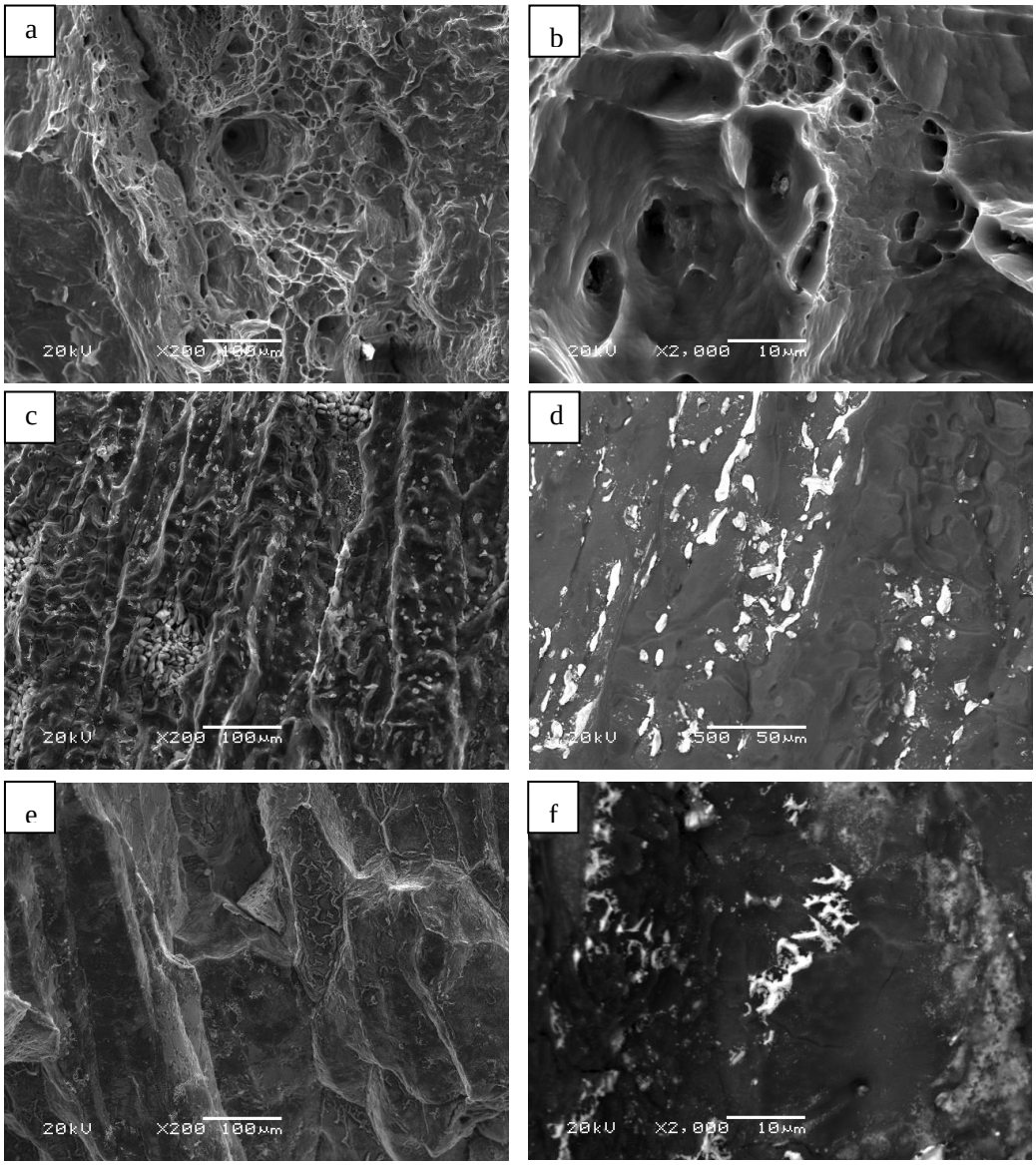


Fig. 2 Fracture surfaces of different alloys: (a), (b) Al-2Li alloy; (c), (d) Al-6GIS alloy; (e), (f) Al-2Li-6GIS alloy.

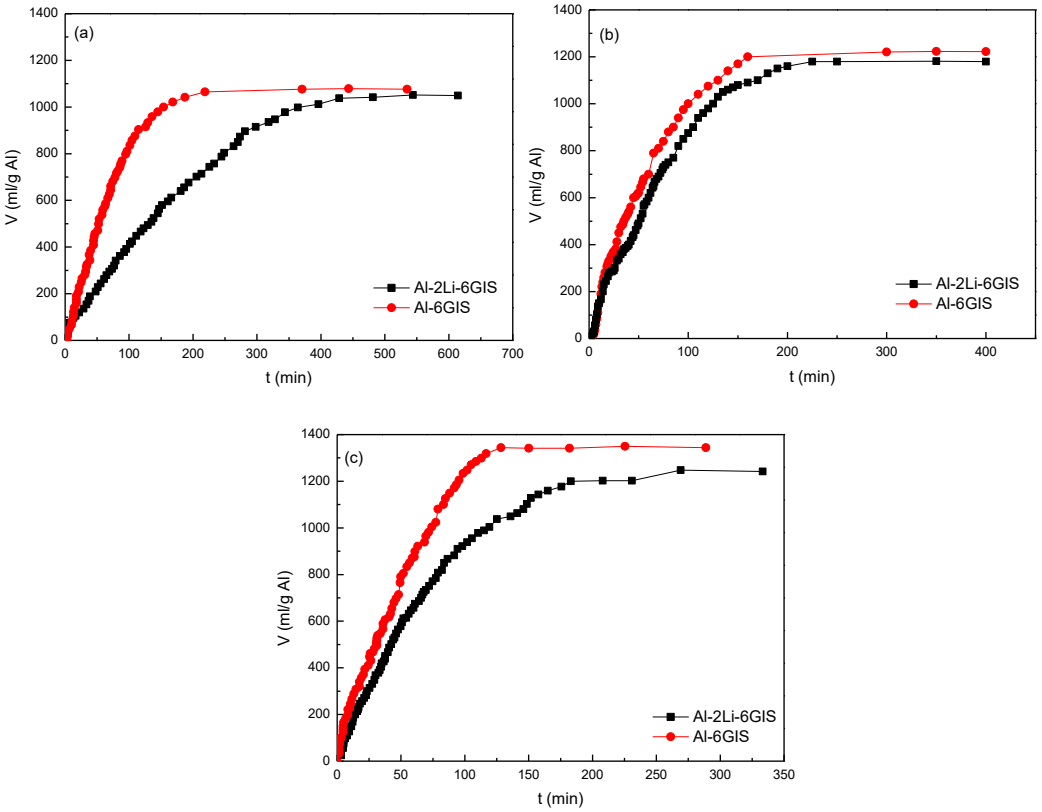


Fig. 3 $H_2$ production curves of the Al-6GIS alloy and Al-2Li-6GIS alloy measured at different water temperatures: (a) 50 °C; (b) 60 °C; (c) 70 °C.

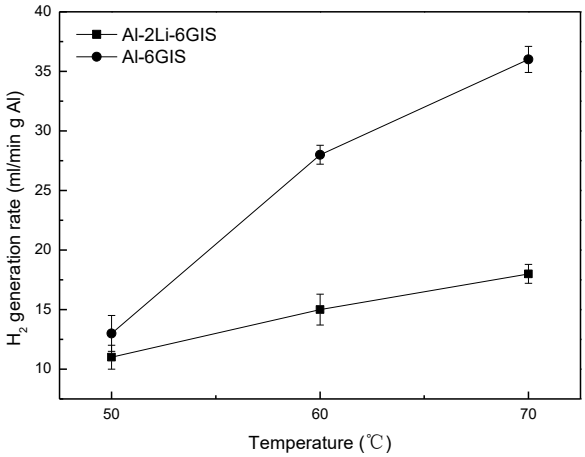


Fig. 4 $H_2$ generation rates of the alloys at different water temperatures.

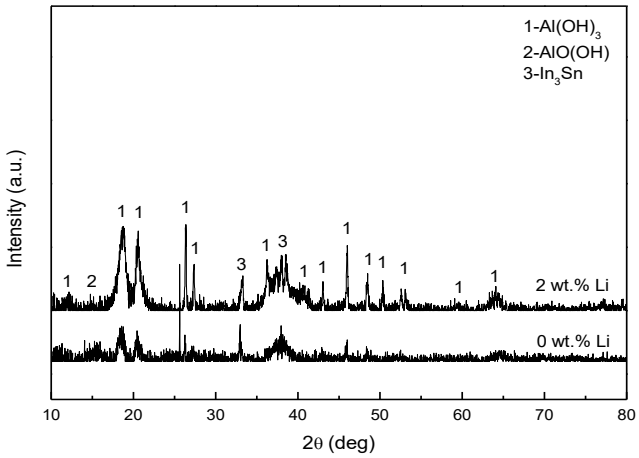


Fig. 5 XRD patterns of the byproducts of the Al-6GIS alloy and Al-2Li-6GIS alloy after the reaction with water at 60 °C.

Table 1 Nominal compositions of the prepared alloy ingots (wt.%).

| Sample | Element (wt.%) | | | | |
|---|---|---|---|---|---|
| | Al | Ga | In | Sn | Li |
| Al -2Li alloy | 98 | 0 | 0 | 0 | 2 |
| Al-6GIS alloy | 94 | 3.8 | 1.5 | 0.7 | 0 |
| Al-2Li-6GIS alloy | 92 | 3.8 | 1.5 | 0.7 | 2 |

Table 2 Compositions of the alloys obtained using EDX.

| Sample | Spectrum | Phase | Element (at.%) | | | | |
|---|---|---|---|---|---|---|---|
| | | | Al | Ga | In | Sn | O |
| Al-2Li alloy | 1 | G | 100.00 | 0.00 | 0.00 | 0.00 | 0.00 |
| Al-6GIS alloy | 2 | G | 57.65 | 1.02 | 0.00 | 0.00 | 41.33 |
| | 3 | GB | 35.57 | 4.63 | 6.04 | 3.62 | 50.14 |
| Al-2Li-6GIS alloy | 4 | G | 55.21 | 3.26 | 0.00 | 0.00 | 41.23 |
| | 5 | GB | 28.59 | 2.44 | 21.72 | 3.54 | 43.71 |

G: Al grain, GB: phase (bright white regions).

Table 3 $H_2$ yields of the alloys at different water temperatures (%).

| Sample | 50 ℃ | 60 ℃ | 70 ℃ |
|---|---|---|---|
| Al-6GIS alloy | 86% | 99% | 100% |
| Al-2Li-6GIS alloy | 84% | 94% | 100% |